BIOCHEMISTRY
including biophysical chemistry & molecular biology

Article

pubs.acs.org/biochemistry

# Spectroscopic Studies of the *Salmonella enterica* Adenosyltransferase Enzyme *Se*CobA: Molecular-Level Insight into the Mechanism of Substrate Cob(II)alamin Activation

Ivan G. Pallares,[†] Theodore C. Moore,[‡] Jorge C. Escalante-Semerena,[‡] and Thomas C. Brunold*[,†]

[†]Department of Chemistry, University of Wisconsin—Madison, Madison, Wisconsin 53706, United States

[‡]Department of Microbiology, University of Georgia, Athens, Georgia 30602, United States

Supporting Information

**ABSTRACT:** CobA from *Salmonella enterica* (*Se*CobA) is a member of the family of ATP:Co(I)rrinoid adenosyltransferase (ACAT) enzymes that participate in the biosynthesis of adenosylcobalamin by catalyzing the transfer of the adenosyl group from an ATP molecule to a reactive Co(I)rrinoid species transiently generated in the enzyme active site. This reaction is thermodynamically challenging, as the reduction potential of the Co(II)rrinoid precursor in solution is far more negative than that of available reducing agents in the cell (e.g., flavodoxin), precluding nonenzymic reduction to the Co(I) oxidation state. However, in the active sites of ACATs, the Co(II)/Co(I) redox potential is increased by >250 mV via the formation of a unique four-coordinate (4c) Co(II)rrinoid species. In the case of the *Se*CobA ACAT, crystallographic and kinetic studies have revealed that the phenylalanine 91 (F91) and tryptophan 93 (W93) residues are critical for *in vivo* activity, presumably by blocking access to the lower axial ligand site of the Co(II)rrinoid substrate. To further assess the importance of the F91 and W93 residues with respect to enzymatic function, we have characterized various *Se*CobA active-site variants using electronic absorption, magnetic circular dichroism, and electron paramagnetic resonance spectroscopies. Our data provide unprecedented insight into the mechanism by which *Se*CobA converts the Co(II)rrinoid substrate to 4c species, with the hydrophobicity, size, and ability to participate in offset $\pi$-stacking interactions of key active-site residues all being critical for activity. The structural changes that occur upon Co(II)rrinoid binding also appear to be crucial for properly orienting the transiently generated Co(I) "supernucleophile" for rapid reaction with cosubstrate ATP.

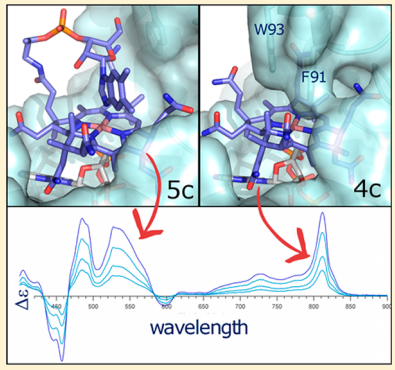


Adenosylcobalamin (AdoCbl) is one of Nature's most complex cofactors, employed by biological systems as a controlled source of radical species.[1,2] It is composed of a redox-active cobalt ion coordinated equatorially by the four nitrogen atoms of a tetrapyrrole macrocycle known as the corrin ring. A pendant 5,6-dimethylbenzimidazole (DMB) base attached to the corrin macrocycle by an intramolecular loop occupies the "lower" (Co$\alpha$) axial position, while an ATP-derived 5′-deoxyadenosyl moiety is bound to the Co ion in the upper (Co$\beta$) position via a unique organometallic bond (Figure 1).[3] AdoCbl serves as the cofactor for a class of enzymes that catalyze various 1,2-rearrangement reactions.[4] These AdoCbl-dependent enzymes can be grouped into three families: (i) enzymes that form aldehydes via dehydration or deamination of substrates, which include diol dehydratase, glycerol dehydratase, and ethanolamine ammonia lyase;[5,6] (ii) aminomutases, such as D-ornithine 4,5-aminomutase and L-leucine 2,3-aminomutase, which facilitate the migration of primary amine groups;[7] and (iii) mutases, such as methylmalonyl-CoA mutase and glutamate mutase, which catalyze carbon skeleton rearrangements.[8,9] A common feature shared by all of these enzymes is the controlled homolytic cleavage of the Co−C(Ado) bond of AdoCbl in response to substrate binding, to yield a reactive Ado-based radical capable of abstracting a hydrogen atom from the substrate.[4]

While only some bacteria and archaea possess the complete enzymatic machinery to synthesize AdoCbl from small molecule precursors, all organisms that require AdoCbl in their metabolism must produce ATP:Co(I)rrinoid adenosyltransferase (ACAT) enzymes.[10] ACATs catalyze the formation of the Co−C(Ado) bond via the transfer of the 5′-deoxyadenosyl moiety of ATP to a cobalamin substrate.[11] To date, three nonhomologous, structurally distinct classes of ACATs have been identified and classified according to their roles in *Salmonella enterica* sv Typhimurium LT2 (hereafter *S. enterica*), which contains a member of each class in its genome.[12−14] The *S. enterica* CobA (*Se*CobA) enzyme is involved in the *de novo* synthetic pathway of AdoCbl and in scavenging various corrinoids from the environment. One prominent substrate for *Se*CobA is cob(II)inamide [Co(II)-Cbi$^+$], which features the cobalt-containing, tetrapyrrolic corrin ring present in all corrinoids but lacks the nucleotide loop and

**Received:** September 22, 2014
**Revised:** November 4, 2014
**Published:** November 25, 2014

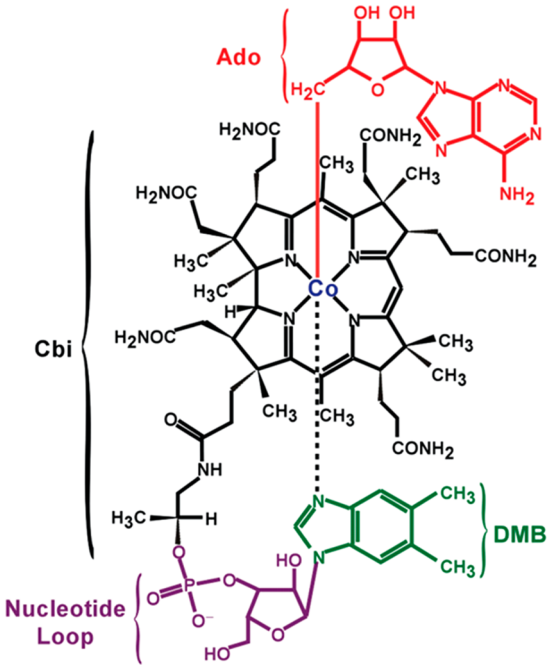


**Figure 1.** Chemical structure of adenosylcobalamin (AdoCbl), the final product of the reaction catalyzed by ATP:Co(I)rrinoid adenosyltransferases (ACATs). In the case of adenosylcobinamide ($AdoCbi^+$) and related species, the DMB moiety and nucleotide loop are absent.

DMB base found in Co(II)Cbl and instead binds a water molecule in the (Co$\alpha$) axial position (Figure 1 and Figure S8 of the Supporting Information).[12] Corrinoids such as cobinamide must be adenosylated before they can be converted to cobalamins, and thus, the *cobA* gene is constitutively expressed by the cell to maintain basal levels of AdoCbl.[12] Alternatively, the gene encoding the PduO ACAT is expressed only when 1,2-propanediol is present, whereas expression of the gene encoding EutT requires the presence of ethanolamine and AdoCbl.[15−17] Note that the single ACAT employed by humans (generally termed hATR) is homologous to the PduO enzyme, and malfunctioning of hATR has been linked to diseases related to cobalamin deficiency, such as methylmalonic aciduria.[18−21]

Previous studies of ACATs have led to the proposal that these enzymes employ a common mechanism for the biosynthesis of AdoCbl.[22] This mechanism involves the one-electron reduction of a Co(II)rrinoid precursor to form a "supernucleophilic" Co(I) species,[23] which performs a nucleophilic attack on the 5′-carbon of ATP to yield the adenosylated product (Figure 2).[11,24] The reduction of Co(II)rrinoid to produce the key Co(I) intermediate is thermodynamically challenging, as the Co(II)/Co(I) reduction potential for the naturally encountered substrates {$E^0$ = −610 mV vs NHE for cob(II)alamin [Co(II)Cbl], and $E^0$ = −490 mV vs NHE for cob(II)inamide [$Co(II)Cbi^+$], a Co(II)Cbl precursor missing the nucleotide loop and DMB base]}[25] is too negative for the reducing agents available in the cell (the semiquinone/reduced flavin couple in FldA, the purported physiological partner to at least one ACAT, CobA, is $E^0$ = −440 mV vs NHE).[26−28] Early spectroscopic studies of *Se*CobA, as well as of the *Lactobacillus reuteri* PduO-type ACAT (*Lr*PduO), have provided strong evidence of the formation of a structurally unique Co(II)rrinoid species in the active sites of these enzymes.[24,29−31] In particular, electron paramagnetic resonance (EPR) characterization of Co(II)rrinoids bound to these enzymes complexed with ATP revealed unusually large $g$ shifts and $A$(Co) hyperfine coupling constants, consistent with the Co(II) ion residing in an effectively square planar, four-coordinate (4c) ligand environment.[24,29] Formation of a 4c intermediate was shown to stabilize the singly occupied redox-active Co $3d_{z^2}$-based molecular orbital and thus to raise the reduction potential by an estimated ≥250 mV, to within the range of those of biologically available reductants.[23,24] Further evidence of enzymatic tuning of the Co(II)/Co(I) redox potential was obtained from magnetic circular dichroism (MCD) studies, which revealed the appearance of a series of sharp, positively signed features between ∼10000 and 20000 $cm^{-1}$ when $Co(II)Cbi^+$ binds to *Se*CobA/ATP or *Lr*PduO/ATP that are unique among Co(II)rrinoid species.[32]

Subsequent crystallographic studies confirmed the presence of 4c Co(II)Cbl species bound to the active sites of *Se*CobA and *Lr*PudO in the presence of ATP and provided insights into the mechanism by which ACATs generate 4c Co(II)rrinoids. Specifically, it was found that a noncoordinating Phe residue occupies the lower axial position of the Co(II)Cbl cofactor where the DMB ligand would normally be found (F112 in *Lr*PudO[33] and F91 in *Se*CobA[34]). A subsequent kinetic and spectroscopic study of *Lr*PduO revealed that F112 and adjacent F187 and V186 residues form a hydrophobic "wall" in response

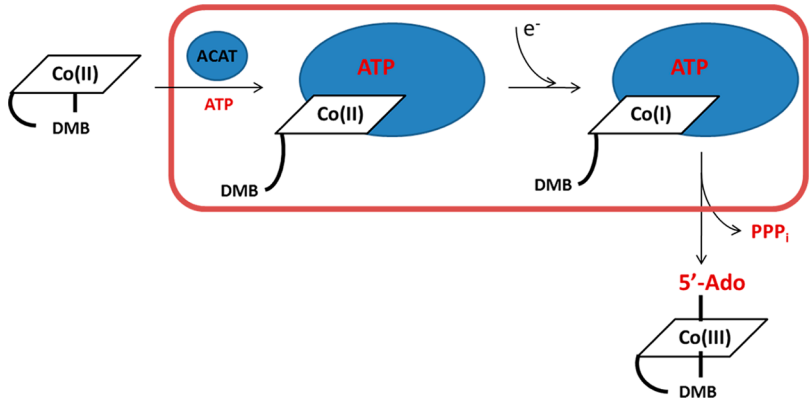


**Figure 2.** Proposed mechanism for the reaction catalyzed by ACATs, adapted from refs 24 and 67. Complexation of the enzyme active site with cosubstrate ATP promotes the binding of Co(II)Cbl and its conversion to a 4c species via removal of the axial ligand. One-electron reduction of this species produces a Co(I)Cbl intermediate that is properly oriented for nucleophilic attack on the 5′-carbon of ATP to form AdoCbl.


dx.doi.org/10.1021/bi5011877 | *Biochemistry* 2014, 53, 7969−7982

to Co(II)rrinoid binding, blocking ligand access to the Co$\alpha$ face of the corrin ring,[35] while a salt bridge interaction between residues D35 and R128 near the corrin ring was found to be important for properly positioning the Co(II)rrinoid substrate.[30] Although the detailed mechanism of 4c Co(II)rrinoid formation employed by *Se*CobA is less well understood, the most recently published X-ray crystal structure of this enzyme provided similar information about the conformation of the active site during catalysis. Notably, this structure revealed the active-site geometry at the catalytic site containing 4c Co(II)Cbl species (the "closed" conformation), as well as the binding geometry of pentacoordinate (5c) Co(II)Cbl prior to enzyme activation (the "open" conformation).[32] It also confirmed the unique binding motif of ATP,[36] oriented toward the corrin ring for nucleophilic attack by the Co ion, and identified additional amino acid residues responsible for displacing the lower axial ligand of the bound corrinoid in the "closed" conformation of the enzyme. In analogy to the previously characterized *Lr*PduO ACAT, a set of hydrophobic residues, namely, F91, W93, V13, and V17, in *Se*CobA are positioned near the lower face of the cofactor, thus providing a wall of hydrophobic residues between the Co(II) ion and the solvent. However, unlike in *Lr*PduO where a single aromatic residue is present at the location where the DMB coordinates to the Co(II) ion in solution,[37,52] two bulky, aromatic amino acids in an offset $\pi$-stacking conformation are positioned at this location in *Se*CobA (Figure 3). This pair of residues is adjacent only to the V13 and V17 residues of the N-terminal helix that caps the active site, while the remaining interactions are with solvent molecules and pendant groups from the corrin ring. Preliminary studies of the *Methanosarcina mazei* CobA enzyme, a *Se*CobA homologue lacking the N-terminal helix, revealed that these Val residues are important for increasing the yield of 4c Co(II)rrinoid species but are not essential for activity.[18] Alternatively, amino acid substitutions at the F91 and W93 positions were shown to have a drastic effect on the catalytic efficiency of *Se*CobA.[32]

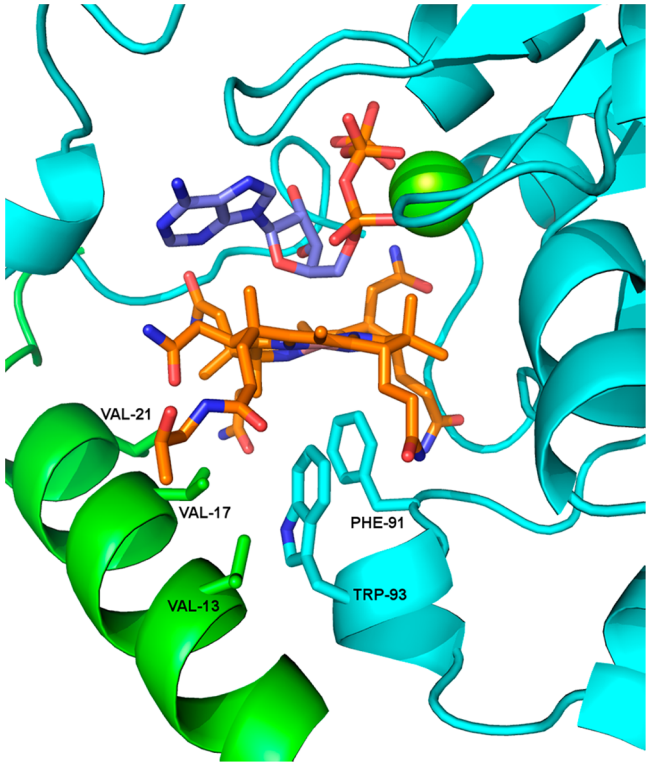


**Figure 3.** X-ray crystal structure of the "closed" subunit of *Se*CobA in the region of the active site featuring 4c Co(II)Cbl (orange), cosubstrate ATP (purple), and Mg(II) (green), based on Protein Data Bank entry 4HUT. The subunit containing the F91 and W93 residues (shown as sticks) is colored cyan. The N-terminal helix of the adjacent "open" subunit, which caps the active site and contains the V13, V17, and V21 residues, is colored green.

Previously, we have employed MCD and EPR spectroscopies to probe the coordination environment of the Co center in Co(II)rrinoids[38,39] and to monitor the structural changes that occur in the catalytic cycles of various cobalamin-dependent enzymes and ACATs.[29−32] MCD spectroscopy offers a particularly sensitive probe of Co(II)rrinoid species formed during enzymatic turnover, as with this technique ligand field (LF) and charge transfer (CT) transitions can be observed that are masked by intense corrin $\pi-\pi^*$ transitions in the corresponding absorption spectra. In the study presented here, we have used electronic absorption, MCD, and EPR spectroscopies to characterize several *Se*CobA variants with substitutions of residues F91 and W93. These variants were chosen to assess the importance of specific intermolecular interactions with respect to the formation of 4c Co(II)rrinoids by varying the size of residues 91 and 93 (F91Y, W93F, F91W, and W93A), their relative positioning (F91W/W93F), and polarity (F91Y and W93H). By conducting studies with Co(II)Cbl and Co(II)Cbi$^+$, both of which are substrates of the enzyme *in vivo* but differ with respect to the identity of the axial ligand to the Co(II) ion,[34,40,41] we have gained significant insights into how the strength of the axial ligand−Co bonding interaction modulates the relative yield of 4c Co(II)rrinoid species in *Se*CobA.

## MATERIALS AND METHODS

**Cofactors and Chemicals.** The chloride salt of aquacobalamin ($[H_2OCbl]Cl$), dicyanocobinamide $[(CN)_2Cbi]$, and potassium formate (HCOOK) were purchased from Sigma and used as obtained. Diaquacobinamide $\{[(H_2O)_2Cbi]^{2+}\}$ was prepared by adding $NaBH_4$ to an aqueous solution of $(CN)_2Cbi$, loading the reaction mixture on a C18 SepPack column, washing it with doubly distilled $H_2O$, and eluting the product with methanol, as described in previous reports.[24,30] Co(II)Cbl and Co(II)Cbi$^+$ were prepared by adding a small volume of saturated HCOOK to degassed solutions of $H_2OCbl^+$ and $(H_2O)_2Cbi^{2+}$, respectively, and the progress of the reduction was monitored spectrophotometrically.

**Protein Preparation and Purification.** Wild-type and variant CobA from *S. enterica* sv. Typhimurium LT2 was purified as described elsewhere.[34] Briefly, the wild-type *cobA* gene was cloned into the pTEV5 overexpression plasmid,[42] which includes a cleavable, N-terminal hexahistidine tag. *Se*CobA variants were generated using the QuikChange II site-directed mutagenesis kit (Stratagene). All proteins were overexpressed in *Escherichia coli* BL21 and purified on a HisTrap nickel affinity column (GE Life Sciences). The N-terminal hexahistidine tag was cleaved using recombinant tobacco etch virus (rTEV) protease.[43] Proteins were purified to homogeneity as determined by sodium dodecyl sulfate−polyacrylamide gel electrophoresis (SDS−PAGE).[44]

**Sample Preparation.** Purified ∼300−500 $\mu$M *Se*CobA in 50 mM Tris buffer (pH 8) containing 0.5 mM DTT was


dx.doi.org/10.1021/bi5011877 | *Biochemistry* 2014, 53, 7969−7982

complexed with Co(II)Cbl or Co(II)Cbi$^+$ under anoxic conditions in an ~0.8:1 cofactor:protein ratio (see the Supporting Information for details). If appropriate, MgATP was added in a 10-fold molar excess over protein as the source of ATP. Solutions were then injected into the appropriate sample cells in an oxygen-free glovebox. Samples were immediately frozen and stored in liquid nitrogen.

**Spectroscopy.** Magnetic circular dichroism (MCD) spectra were collected on a Jasco J-715 spectropolarimeter in conjunction with an Oxford Instruments SM-4000 8T magnetocryostat. All MCD spectra were obtained by taking the difference between spectra collected with the magnetic field oriented parallel and antiparallel to the light propagation axis to remove contributions from the natural CD and glass strain. X-Band EPR spectra were obtained by using a Bruker ESP 300E spectrometer in conjunction with an Oxford ESR 900 continuous-flow liquid helium cryostat and an Oxford ITC4 temperature controller. The microwave frequency was measured with a Varian EIP model 625A CW frequency counter. All spectra were collected using a modulation amplitude of 10 G and a modulation frequency of 100 kHz. EPR spectral simulations were performed using the WEPR program developed by F. Neese.

**Computations.** Initial atomic coordinates for the structure of wild-type *Se*CobA in complex with ATP and Co(II)Cbl were obtained from the most recently published crystal structure [Protein Data Bank (PDB) entry 4HUT].[34] Pymol was used to introduce *in silico* amino acid substitutions into the *Se*CobA subunit containing 4c Co(II)Cbl and ATP. The newly introduced residues were positioned so as to minimize steric clashes, while preserving the orientation of the original residue as closely as possible. Molecular mechanics as implemented in GROMACS version 4.5 was then employed to minimize the energy of the protein model in the presence of water solvent [using the simple point charge (SPC) model for water molecules][45] with a box size of 5 nm. The Amber98 force field was used for the protein residues and supplemented with parameters for ATP by Carson et al.[46] and for cobalamin by Marques et al.[47,48] To accelerate the calculations, the other subunit of the *Se*CobA dimer containing 5c Co(II)Cbl was removed, except for the N-terminal helix that interacts with the subunit of interest. No significant differences in the secondary structure were observed among the energy-minimized models of the variants, and computed Ramachandran plots for the optimized structures indicated that no misoriented amino acids or unreasonable conformations were present. From these optimized structures, the residues at positions 91 and 93 were excised and used in subsequent density functional theory (DFT) single-point calculations with Orca version 3.0 to evaluate the magnitude of dispersion interactions involving these two residues (while ignoring all other residues). These computations employed the B3LYP functional and TZVP basis set for all atoms and were conducted by choosing the dispersion correction developed by Grimme and co-workers.[49−52] Although the absolute dispersion energies obtained in these calculations may be subject to systematic errors because substitutions of residues 91 and 93 may also alter the interactions with nearby amino acid residues, the computed values should properly reproduce the general trend in dispersion energies.

## RESULTS

**Corrinoid Binding to Wild-Type *Se*CobA (*Se*CobA$^{WT}$).** The low-temperature (LT) absorption spectrum of Co(II)Cbi$^+$ (Figure 4A, gray trace) is characterized by an intense feature

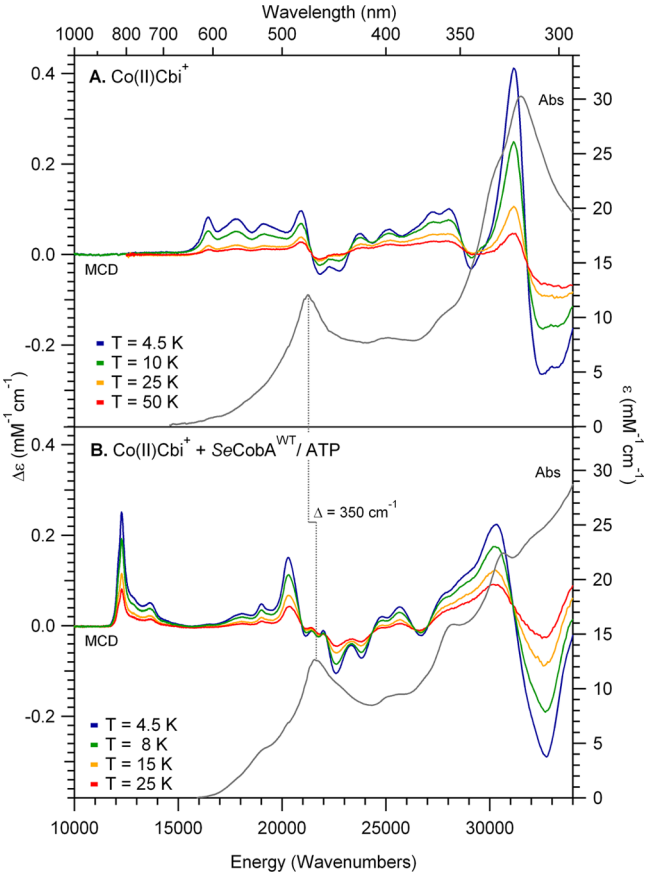


**Figure 4.** Absorption spectra collected at 4.5 K (gray traces) and variable-temperature MCD spectra at 7 T of (A) free Co(II)Cbi$^+$ and (B) Co(II)Cbi$^+$ in the presence of *Se*CobA$^{WT}$ and ATP.

centered at ~21000 cm$^{-1}$, the so-called $\alpha$-band that has previously been assigned to a corrin-based $\pi \rightarrow \pi^*$ transition on the basis of its high extinction coefficient and time-dependent DFT results.[53,54] This feature is blue-shifted by ~150 cm$^{-1}$ from its position in the absorption spectrum of Co(II)Cbl (Figure 5A, gray trace), as reported previously.[38] In the presence of the *Se*CobA$^{WT}$/ATP complex (Figure 4B, gray trace), the $\alpha$-band undergoes a further (~350 cm$^{-1}$) shift to a higher energy. As the strength of the metal−ligand interaction in Co(II)rrinoids was previously found to modulate the relative energies of the corrin $\pi/\pi^*$ frontier molecular orbitals (MOs),[39] the observed blue-shift of the $\alpha$-band is consistent with large perturbations to the axial ligand environment of Co(II)Cbi$^+$ in the presence of the *Se*CobA$^{WT}$/ATP complex. Further insight into the nature of these perturbations is obtained by MCD spectroscopy. Most importantly, a series of sharp, positively signed intense bands appear in the low-energy region (~10000 to 20000 cm$^{-1}$) of the MCD spectrum upon binding of Co(II)Cbi$^+$ to the *Se*CobA$^{WT}$/ATP complex (Figure 4B, color traces) that are characteristic of Co(II)rrinoid species bound to ACATs.[29,31,38] From their large MCD:absorption intensity ratios [alternatively, C:D ratios (see Figure S5 of the Supporting Information)] and relatively narrow bandwidths,


dx.doi.org/10.1021/bi5011877 | *Biochemistry* 2014, 53, 7969−7982

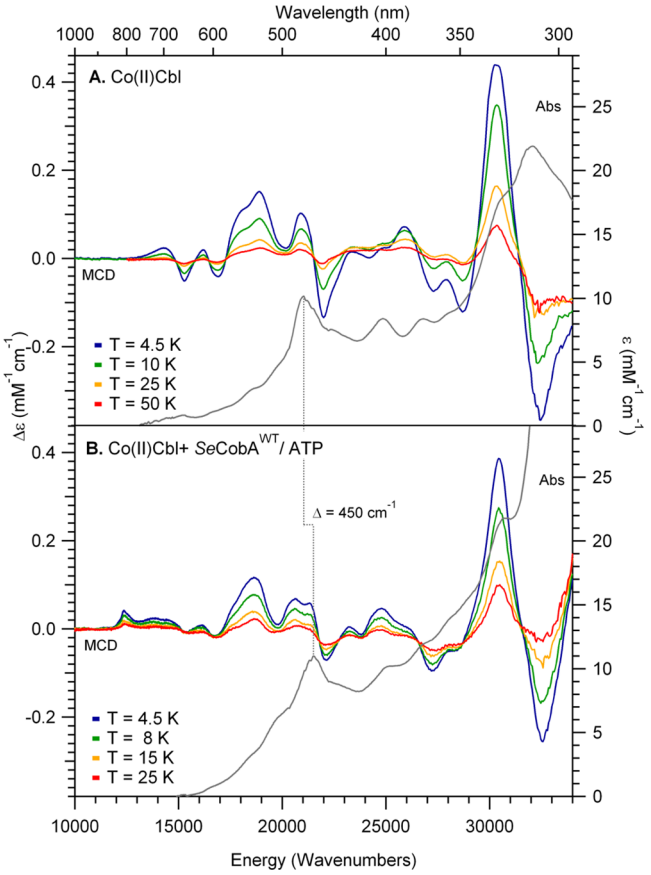


**Figure 5.** Absorption spectra collected at 4.5 K (gray traces) and variable-temperature MCD spectra at 7 T of (A) free Co(II)Cbl and (B) Co(II)Cbl in the presence of *Se*CobA$^{WT}$ and ATP.

the features at 12300 cm$^{-1}$ ($\delta$-band) and 13600 cm$^{-1}$ ($\beta$-band) have been assigned to the electronic origin and vibrational sideband of a single LF transition.[24] These features are red-shifted from their counterparts in the free Co(II)Cbi$^+$ MCD spectrum by ~4000 cm$^{-1}$ (Figure 4A, color traces), consistent with the formation of an essentially 4c Co(II)rrinoid species.[24,29,33] As no spectroscopic features from five-coordinate (5c) Co(II)rrinoid species are observed in this region of the spectrum, the intensity of the $\delta$-band can been used to estimate the relative yield of 4c Co(II)rrinoid species generated by ACATs.[30] In the case of Co(II)Cbi$^+$ bound to *Se*CobA$^{WT}$, the intensity of the $\delta$-band relative to that of the 16400 cm$^{-1}$ feature of 5c Co(II)Cbi$^+$ indicates that the 4c yield is ~50% (Table 4). Additionally, a sharp positive feature is observed at 19000 cm$^{-1}$ ($\lambda$-band), alongside an intense positive band at 20300 cm$^{-1}$ ($\sigma$-band). Because these features are found at energies lower than that of the $\alpha$-band, the lowest-energy corrin-based $\pi \rightarrow \pi^*$ transition observed for Co(II)-rrinoids,[31,55] and given their modest C:D ratios and high MCD intensities, they can be attributed to electronic transitions with significant CT character. The bands observed at higher energies have been assigned primarily to corrin $\pi \rightarrow \pi^*$ transitions on the basis of their small C:D ratios and low MCD intensities.[30,38] Although the relative intensities of these features vary significantly among Co(II)rrinoid species (Figure S6 of the Supporting Information), establishing specific band assignments becomes difficult because of the presence of multiple electronic transitions of varied LF, CT, and $\pi \rightarrow \pi^*$ character expected in this region of the spectrum.

As in the case of Co(II)Cbi$^+$, the absorption spectrum of Co(II)Cbl also changes in the presence of the *Se*CobA$^{WT}$/ATP complex, with the $\alpha$-band undergoing an ~450 cm$^{-1}$ blue-shift (Figure 5, gray traces). Intriguingly, in the MCD spectrum of Co(II)Cbl and the *Se*CobA$^{WT}$/ATP complex, the intensity of the $\delta$-band is considerably weaker than in the analogous Co(II)Cbi$^+$ spectrum (Figure 5B), indicating a large (~5-fold) decrease in the relative yield of 4c species when Co(II)Cbl serves as the substrate of *Se*CobA$^{WT}$. Thus, the magnitude of the blue-shift of the $\alpha$-band observed in the absorption spectrum does not correlate directly with the yield of 4c species formed in the *Se*CobA$^{WT}$ active site, indicating that absorption spectroscopy is not suitable for quantifying the relative yields of 4c Co(II)rrinoid species. A further analysis of the MCD spectrum of Co(II)Cbl and the *Se*CobA$^{WT}$/ATP complex reveals that the remaining spectral contributions are consistent with the presence of a 5c Co(II)Cbl species with N(DMB) bound to the Co(II) ion. However, the MCD features of this 5c species are significantly different from those observed for free Co(II)Cbl. Specifically, the positive feature at ~19000 cm$^{-1}$ in the MCD spectrum of Co(II)Cbl red-shifts by ~200 cm$^{-1}$ in the presence of the *Se*CobA$^{WT}$/ATP complex, while the positive feature at 21000 cm$^{-1}$ blue-shifts by ~400 cm$^{-1}$ (Figure 7, top). Because features in this region of the MCD spectrum of Co(II)Cbl have previously been assigned to LF and CT transitions that are sensitive to changes in the axial ligand environment,[56] the band shifts induced by the addition of the *Se*CobA$^{WT}$/ATP complex are consistent with perturbations to the DMB base via interactions with the protein scaffold. Lastly, the high-energy region (>22000 cm$^{-1}$) of the MCD spectrum of Co(II)Cbl in the presence of the *Se*CobA$^{WT}$/ATP complex is reminiscent of that of free Co(II)Cbl, in particular with regard to the intense derivative-shaped feature at 31000 cm$^{-1}$ (also see Figure S7 of the Supporting Information). Inspection of the remaining bands in this region, however, reveals sizable differences in terms of their positions and relative intensities, suggesting that the conformation of the corrin ring in the 5c Co(II)Cbl fraction is significantly altered from that of free Co(II)Cbl. These results are in agreement with the bond distances and angles of the enzyme-bound 5c and 4c Co(II)Cbl species derived from the most recent crystal structure of *Se*CobA$^{WT}$ (Table 1). A

**Table 1. Relevant Structural Parameters of Free and *Se*CobA-Bound Co(II)Cbl Species As Determined by X-ray Crystallography**

| Co(II)Cbl species | Co−$C_{ATP}$ (Å) | Co−$N_{DMB}$ (Å) | $\theta$(LA) (deg) | $\phi$(SA) (deg) |
|---|---|---|---|---|
| no protein[a] | n/a[c] | 2.13 | 19.8 | 6.3 |
| 5c SeCobA site ("open")[b] | 3.42 | 2.32 | 26.2 | 7.7 |
| 4c SeCobA site ("closed")[b] | 3.06 | n/a[c] | 19.5 | 10.7 |

[a]From ref 57. [b]From PDB entry 4HUT.[34] [c]Not applicable.

comparison of the relevant structural parameters of free Co(II)Cbl[57] and the 5c Co(II)Cbl fraction bound to the *Se*CobA$^{WT}$/ATP complex indicates that the Co−N(DMB) bond length increases by ~0.2 Å upon enzyme binding, concurrent with an ~6° increase in the long axis, butterfly fold angle, $\theta$(LA).[a] Upon removal of the DMB ligand, $\theta$(LA) decreases by ~6°, $\phi$(SA) increases by ~3°, and the Co···5′-C(ATP) distance is shortened by ~0.4 Å, highlighting the effect


dx.doi.org/10.1021/bi5011877 | *Biochemistry* 2014, 53, 7969−7982

of the rearrangement of the F91 and W93 active-site residues on the relative positioning and conformation of the Co(II)-rrinoid substrate.

**Point Substitutions at the W93 Position.** *W93A.* Previous studies have indicated that the tryptophan residue at position 93 (W93) is critical for retaining enzyme activity;[18] thus, it was originally postulated that this residue played a role similar to that of F112 in the *Lr*PduO ACAT. However, the most recent crystal structure of *Se*CobA$^{WT}$ with Co(II)Cbl and MgATP bound shows instead that a nearby phenylalanine (F91) residue is positioned on the face of the corrin ring where the DMB group is usually found. It is possible that the aromatic side chain of the W93 residue is associated with this F91 residue in an offset $\pi$-stacking fashion during catalysis. Because replacement of W93 with alanine completely abolishes the catalytic activity of the enzyme with Co(II)Cbl, while modest activity is retained with Co(I)Cbl,[34] the W93A substitution likely affects the Co(II)/Co(I) reduction step. Indeed, the MCD spectra of Co(II)Cbi$^+$ and Co(II)Cbl in the presence of the *Se*CobA$^{W93A}$/ATP complex are almost identical to the corresponding MCD spectra in the absence of ATP (Figures 6 and 7, trace G) and the MCD spectra of the free cofactors (Figures 6 and 7, trace H), indicating that the variant is unable to generate 4c Co(II)rrinoids.

*W93F.* Substitution of Trp93 with Phe, a smaller planar and nonpolar amino acid, results in a *Se*CobA variant with behavior similar to that of the WT enzyme in Co(II)rrinoid and Co(I)rrinoid *in vitro* assays.[34] Indeed, the MCD spectrum of Co(II)Cbi$^+$ in the presence of the *Se*CobA$^{W93F}$/ATP complex is very similar to that obtained with *Se*CobA$^{WT}$, though the prominent low-energy $\delta$-band at ~12300 cm$^{-1}$ is marginally broadened, suggesting that the Phe residue provides more conformational freedom to the bound corrinoid (Figure 6, traces A and D). A quantitative analysis of this spectrum reveals that a larger fraction of 4c Co(II)Cbi$^+$ species is generated in the variant than in the *Se*CobA$^{WT}$/ATP complex (Table 4D). In contrast, in the MCD spectrum of Co(II)Cbl with the *Se*CobA$^{W93F}$/ATP complex, the intensity of the $\delta$-band is decreased 4-fold from that observed in the presence of *Se*CobA$^{WT}$. The MCD features at 15000 and 20000 cm$^{-1}$ associated with the remaining 5c Co(II)Cbl species are very similar to those observed for the analogous species in *Se*CobA$^{WT}$ and distinct from those displayed by free Co(II)Cbl (Figure 7, traces A and D, bands *a* and *b*). This result indicates that the 5c fraction of Co(II)Cbl is also bound to the *Se*CobA$^{W93F}$/ATP complex and adopts a conformation similar to that of the 5c Co(II)Cbl species in *Se*CobA$^{WT}$. Thus, the decreased yield of 4c Co(II)Cbl species in *Se*CobA$^{W93F}$ can be attributed to the smaller size of the introduced Phe residue relative to the native Trp, which leads to a decreased level of steric crowding when Co(II)Cbl binds to the enzyme active site in the DMB-on form.[30] Because of the weaker interaction of the $H_2O$ ligand with the Co(II) ion in Co(II)Cbi$^+$, the decreased level of steric crowding in the active site of *Se*CobA$^{W93F}$ has a smaller effect on the 4c−5c equilibrium when this species is used as the substrate.

*W93H.* Compared to the results obtained with *Se*CobA$^{W93F}$, the MCD spectrum of Co(II)Cbi$^+$ in the presence of the *Se*CobA$^{W93H}$/ATP complex displays a broadening of the $\delta$- and $\sigma$-bands and a decrease in their intensities. These changes signify a 2-fold decrease in the yield of 4c Co(II)Cbi$^+$, consistent with a less constrained active site upon introduction of the smaller imidazole side chain (Figure 6 and Table 4, E).

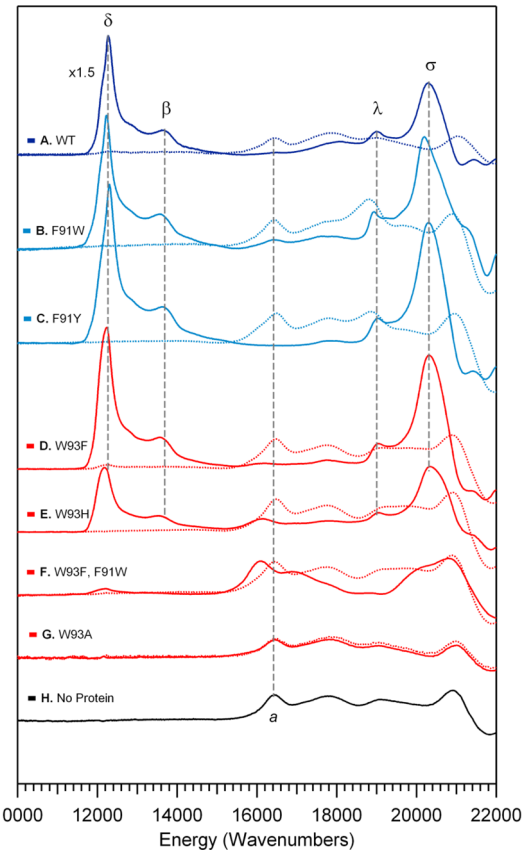


**Figure 6.** MCD spectra at 4.5 K and 7 T of Co(II)Cbi$^+$ obtained in the presence of *Se*CobA$^{WT}$ and various variants. Solid lines show the spectra in the presence of ATP, while dotted lines are the corresponding traces in the absence of ATP. Panels A−G are labeled according the amino acid substitution(s) introduced into *Se*CobA. The primary spectroscopic features due to 4c Co(II)Cbi$^+$ species are labeled with lowercase Greek letters for the *Se*CobA$^{WT}$ spectrum and are highlighted by vertical lines. The relevant MCD feature of free Co(II)Cbi$^+$ (H) is labeled with a lowercase Latin letter, and its position is also highlighted by a vertical line.

As expected from the lower yield of 4c Co(II)Cbi$^+$ in *Se*CobA$^{W93H}$, increased contributions from 5c (i.e., water-bound) Co(II)Cbi$^+$ are observed in the 16000−20000 cm$^{-1}$ region of the MCD spectrum; however, these features are not identical to those seen in the corresponding MCD spectrum in the absence of ATP. In particular, the feature corresponding to the lowest-energy LF transition of Co(II)Cbi$^+$ is red-shifted by ~300 cm$^{-1}$ in the spectrum of the sample containing the *Se*CobA$^{W93H}$/ATP complex (Figure 6E, band *a*), indicating that the 5c Co(II)Cbi$^+$ fraction features an elongated Co−O($H_2$) bond.[24,58] Thus, while a smaller fraction of 4c Co(II)Cbi$^+$ species is generated in *Se*CobA$^{W93H}$ than in the wild-type enzyme, the remaining 5c Co(II)Cbi$^+$ fraction is significantly perturbed upon binding to *Se*CobA$^{W93H}$. The lack of features in the 14000−16000 cm$^{-1}$ region of the MCD spectrum of Co(II)Cbi$^+$ in the presence of SeCobA$^{W93H}$ indicates that the imidazole side chain of H93 does not serve as a ligand to the Co(II) ion, ruling out the possibility that His binding precludes the formation of a 4c species (Figure 6D; see Figure 9 for a comparison to a His-on species). As expected, the W93H substitution has a more dramatic effect on the 4c−5c equilibrium when Co(II)Cbl instead of Co(II)Cbi$^+$ is used as the substrate. In fact, the MCD spectrum of Co(II)Cbl in the


dx.doi.org/10.1021/bi5011877 | *Biochemistry* 2014, 53, 7969−7982

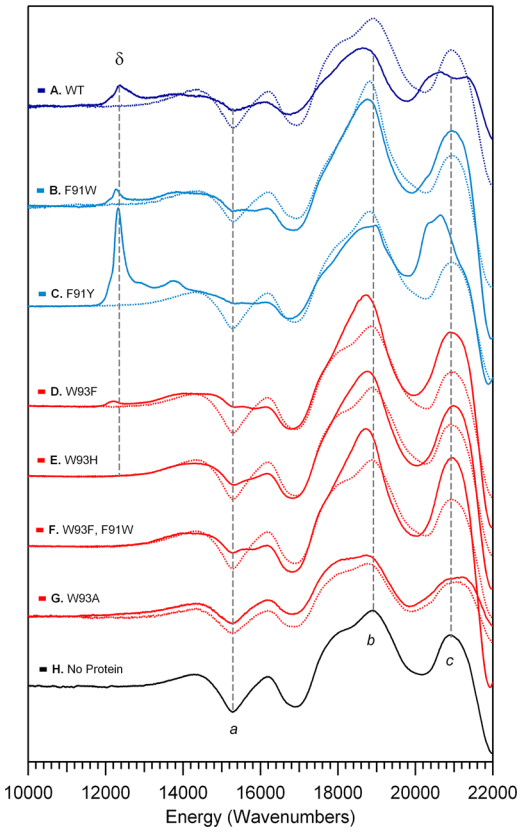


**Figure 7.** MCD spectra at 4.5 K and 7 T of Co(II)Cbl obtained in the presence of *Se*CobA$^{WT}$ and various variants. Solid lines show the spectra in the presence of ATP, while dotted lines are the corresponding traces in the absence of ATP. Panels A–G are labeled according to the amino acid substitution(s) introduced into *Se*CobA. The feature due to 4c Co(II)Cbl species (band $\delta$) is highlighted by a vertical line. The relevant MCD features of free Co(II)Cbl (H) are labeled with lowercase Latin letters, and their positions are also highlighted by vertical lines.

presence of the *Se*CobA$^{W93H}$/ATP complex (Figure 7E) does not contain any discernible contribution from the $\delta$-band transition, while the features at higher energies are analogous to those observed in the presence of *Se*CobA$^{WT}$ and *Se*CobA$^{W93F}$. These findings indicate that the side chain of residue W93 is particularly important for promoting the dissociation of the DMB moiety from the Co(II) ion, as replacement of the native heterocyclic nine-membered indole ring by smaller phenyl and imidazole groups progressively shifts the equilibrium toward 5c Co(II)rrinoid species, inhibiting the formation of 4c Co(II)Cbl in *Se*CobA$^{W93H}$.

**Substitutions of Residue F91.** *F91W.* In the MCD spectrum of Co(II)Cbi$^+$ in the presence of *Se*CobA$^{F91W}$ and ATP, the $\delta$- and $\beta$-bands are as intense as in the spectrum obtained with the *Se*CobA$^{WT}$/ATP complex (Figure 6B). Interestingly, the $\lambda$- and $\sigma$-bands are red-shifted by ~100 cm$^{-1}$ from their positions in the spectra of other *Se*CobA variants capable of generating 4c Co(II)Cbi$^+$. As both of these bands arise from mixed CT and LF transitions of 4c Co(II)Cbi$^+$ that are sensitive to perturbations of the frontier MOs of the corrin ring, these shifts indicate that the conformation of the corrin ring is uniquely perturbed in the active site of the *Se*CobA$^{F91W}$/ATP complex. As in the case of Co(II)Cbi$^+$, the intensity of the $\delta$-band in the MCD spectrum of Co(II)Cbl in the presence of the *Se*CobA$^{F91W}$/ATP complex is comparable to that observed in the spectrum with the *Se*CobA$^{WT}$/ATP complex (Figure 7B). These results conclusively demonstrate that *Se*CobA$^{F91W}$ is capable of generating 4c Co(II)Cbi$^+$ and Co(II)Cbl species with yields approaching those achieved by *Se*CobA$^{WT}$. However, kinetic studies of *Se*CobA$^{F91W}$ with Co(II)Cbl showed catalytic activity diminished relative to that of *Se*CobA$^{WT}$, while the activity with Co(I)Cbl was largely retained, suggesting that the Co(II)/Co(I) reduction step is detrimentally affected by the F91W substitution. These seemingly conflicting results can be reconciled by recognizing that the larger size of the indole group of residue 91 in *Se*CobA$^{F91W}$ relative to the phenyl group in *Se*CobA$^{WT}$ introduces new steric constraints into the active site that affect the orientation of the bound 4c Co(II)rrinoid, as evidenced by the shift in the $\lambda$- and $\sigma$-bands observed spectroscopically. These structural changes could suppress the rate of electron transfer to the Co(II) ion and/or lead to uncontrolled side reactions of the transiently generated Co(I)Cbl "super-nucleophile". While our spectroscopic results suggest that this improper orientation of the Co(II)rrinoid substrate occurs only in the *Se*CobA$^{F91W}$/ATP complex, thus favoring the latter scenario, further experiments are needed to pinpoint the origin of the decreased activity observed for this variant.

*W93F/F91W.* The MCD spectrum of Co(II)Cbi$^+$ in the presence of the *Se*CobA$^{W93F/F91W}$/ATP complex exhibits a very weak and broad $\delta$-band, from which we can estimate that the yield of 4c Co(II)Cbi$^+$ species is reduced more than 10-fold from that achieved by *Se*CobA$^{WT}$ and 20-fold from that of *Se*CobA$^{F91W}$ (Figure 6F). The remaining 5c Co(II)Cbi$^+$ fraction is also bound to the active site of the double variant, but with a perturbed Co–O($H_2$) interaction, as indicated by the ~300 cm$^{-1}$ red-shift of the lowest-energy LF transition near ~16000 cm$^{-1}$ from its position observed for free Co(II)Cbi$^+$ (Figure 6H).[58] As expected from the low yield of 4c Co(II)Cbi$^+$ in the *Se*CobA$^{W93F/F91W}$/ATP complex, the MCD spectrum of Co(II)Cbl in the presence of this variant lacks the $\delta$-band, indicating that no 4c Co(II)Cbl is generated under the experimental conditions used (Figure 7F). Further inspection of this spectrum indicates that the 5c Co(II)Cbl species is significantly perturbed by the enzyme (Figure 7F, bands *a* and *b*), as observed for other *Se*CobA variants capable of generating 4c Co(II)Cbi$^+$.

While our results indicate that the introduction of the F91W and W93F substitutions into *Se*CobA$^{W93F/F91W}$ drastically lowers the yield of 4c Co(II)rrinoid species, this variant was shown to exhibit $k_{cat}$ and $K_M$ values similar to those of *Se*CobA$^{WT}$. Although these observations are difficult to rationalize on the basis of spectroscopic and kinetic data alone, inspection of the *Se*CobA$^{WT}$ crystal structure reveals that residues F91 and W93 are positioned so as to participate in an offset $\pi$-stacking interaction, with the larger W93 side chain occupying the more remote position relative to the corrin ring. Switching the relative positioning of these residues in *Se*CobA$^{W93F/F91W}$ likely causes the Co(II)rrinoid substrates to adopt a different orientation within the enzyme active site, especially at the low temperatures used in our spectroscopic experiments. Under the conditions used to characterize the *Se*CobA$^{F91W/W93F}$ variant kinetically (i.e., in the absence of glycerol and at 298 K), the enhanced thermal motion of residues 91 and 93 may cause the active site to adopt a more wild-type-like conformation, resulting in $k_{cat}$ and $K_M$ values similar to those of *Se*CobA$^{WT}$.


dx.doi.org/10.1021/bi5011877 | *Biochemistry* 2014, 53, 7969–7982

*F91H*. The MCD spectrum of Co(II)Cbi$^+$ in the presence of ATP-free *Se*CobA$^{F91H}$ lacks any contributions from 4c Co(II)-rrinoid species and instead is very similar to the MCD spectrum of free Co(II)Cbl (Figure 9B). As the nucleotide loop and terminal DMB group are absent in Co(II)Cbi$^+$, the characteristic spectroscopic features of nitrogen ligation observed in the MCD spectrum of Co(II)Cbi$^+$ in the presence of *Se*CobA$^{F91H}$ indicate that the newly introduced H91 residue can coordinate to the Co(II) ion. The corresponding EPR spectrum reveals that 50% of the Co(II)Cbi$^+$ substrate is present in the His-on state (Figure 8B), while the remaining fraction retains the water ligand (Table 2, B). Upon addition of ATP to this complex, the positively signed MCD features at 17500 and 18700 cm$^{-1}$ red-shift by ~500 cm$^{-1}$, while the lower-energy derivative-shaped features are replaced by an unprecedented set of weak positive bands above 13300 cm$^{-1}$ (Figure 9C). The EPR spectrum obtained for this species indicates that ~100% of Co(II)Cbi$^+$ is now present with nitrogen ligation from H91 (Figure 8C), as evidenced by the observed superhyperfine splittings due to $^{14}$N ($I$ = 1) and the absence of features reminiscent of Co(II)Cbi$^+$ (Figure 8C). The observed $g$ values decrease significantly in response to His binding (Table 3, A and C), consistent with a further destabilization of the singly occupied Co $3d_{z^2}$-based MO caused by the increase in the extent of axial $\sigma$-antibonding interaction upon $H_2O$ → His ligand substitution. Interestingly, the $A_z(^{59}Co)$ value for the His-bound Co(II)Cbi$^+$ species in *Se*CobA$^{F91H}$ is 130 MHz smaller than for free Co(II)Cbl, which may be due to the covalency of the Co−N(His) bond being larger than that of the Co−N(DMB) bond, or a tilting of the His ligand relative to the corrin ring (Figure 8 and Table 3, A and C).[38] The hyperfine structure is much better resolved in the EPR spectrum of the His-on Co(II)Cbi$^+$ species than in the Co(II)Cbl spectrum (Figure 9C,D), indicating a markedly decreased conformational heterogeneity of the axial ligand. These findings suggest that the protein scaffold imposes a particular conformation on the His residue, possibly via H-bonding or via offset $\pi$-stacking interactions with nearby amino acids.

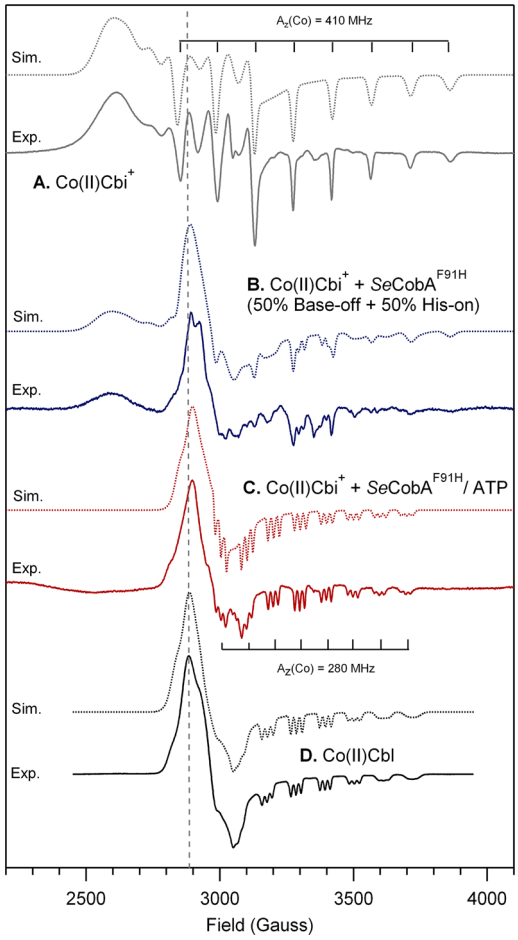


**Figure 8.** X-Band EPR spectra collected at 40 K of (A) free Co(II)Cbi$^+$, (B) Co(II)Cbi$^+$ in the presence of *Se*CobA$^{F91H}$, and (C) Co(II)Cbi$^+$ in the presence of *Se*CobA$^{F91H}$ and ATP. For reference, the spectrum of free Co(II)Cbl is shown in panel D, with the most intense feature highlighted by a dashed line. EPR spectra were collected using a 9.36 GHz microwave source, a 2 mW microwave power, a 5 G modulation amplitude, a 100 kHz modulation frequency, and a 328 ms time constant. Spectra were simulated using the parameters provided in Table 2.

*F91Y*. The MCD spectrum of Co(II)Cbi$^+$ in the presence of the *Se*CobA$^{F91Y}$/ATP complex is strikingly similar to that obtained with the *Se*CobA$^{WT}$/ATP complex, though the $\delta$-, $\beta$-, $\lambda$-, and $\sigma$-bands associated with the 4c Co(II)Cbi$^+$ fraction are considerably more intense. Additionally, the features at ~15000 cm$^{-1}$ due to 5c Co(II)Cbi$^+$ are notably absent in the variant spectrum, indicating that introduction of a Tyr residue at position 91 results in a nearly complete conversion of enzyme-bound Co(II)Cbi$^+$ to a 4c species (Table 4, C). Similarly, the MCD spectrum of Co(II)Cbl in the presence of the *Se*CobA$^{F91Y}$/ATP complex reveals a 5-fold increase in the yield of 4c species relative to that achieved by the *Se*CobA$^{WT}$ enzyme (Table 4, C, and Figure 7C). Thus, even though the relative yield of 4c Co(II)rrinoid species generated by *Se*CobA$^{F91Y}$ remains ~50% lower when Co(II)Cbl instead of Co(II)Cbi$^+$ is used as the substrate, this variant is much more effective at generating 4c Co(II)rrinoid species than *Se*CobA$^{WT}$. Consistent with these results, *Se*CobA$^{F91Y}$ was found to have a 3-fold larger $k_{cat}$ and a 6-fold lower $K_M$ compared to those of *Se*CobA$^{WT}$ when Co(II)Cbl was used as the substrate.[34]

## DISCUSSION

More than 25 enzymes are required for the complete biosynthesis of AdoCbl by prokaryotes. A critical step in this *de novo* pathway involves the attachment of a 5′-deoxyadenosyl (Ado) group to the cobalt ion on the Co$\beta$ face, carried out by the *Se*CobA ACAT in *S. enterica*.[24] While no eukaryotes are known to synthesize AdoCbl *de novo*, they retain genes encoding ACAT enzymes in their genomes. For example, the human ACAT, hATR, converts Co(II)Cbl to AdoCbl and delivers it to the methylmalonyl-CoA mutase (MMCM) enzyme to restore catalytic activity following cofactor deactivation.[21,32,59] Intriguingly, the three distinct families of known ACATs seem to employ the same general catalytic mechanism, even though they share little primary sequence homology and differ with respect to the morphology of the corrinoid binding site.[11,24,29] While a recent report has highlighted the molecular interactions that are critical for the catalytic activity of the *Lr*PduO ACAT,[30] a homologue of hATR, the roles of individual active-site residues in the remaining ACAT families have not yet been elucidated. To enhance our current understanding of the mechanism by which *Se*CobA and related ACATs catalyze the Ado group transfer from ATP to Co(II)rrinoid substrates, we have employed MCD spectroscopy to monitor the effects of active-site amino


dx.doi.org/10.1021/bi5011877 | *Biochemistry* 2014, 53, 7969−7982

Table 2. EPR Parameters for Co(II)Cbi$^+$ in the Absence and Presence of the *Se*CobA$^{F91H}$/ATP Complex[a]

| | $g$ values | | | $A(^{59}Co)$ (MHz) | | | $A(^{14}N)$ (MHz) | | |
|---|---|---|---|---|---|---|---|---|---|
| | $g_z$ | $g_y$ | $g_x$ | $A_z$ | $A_y$ | $A_x$ | $A_z$ | $A_y$ | $A_x$ |
| (A) Co(II)Cbi$^+$ | 2.002 | 2.345 | 2.335 | 410 | 240 | 240 | n/a[b] | n/a[b] | n/a[b] |
| (B) Co(II)Cbi$^+$/*Se*CobA$^{F91H}$ | | | | | | | | | |
| base-off | 2.002 | 2.365 | 2.335 | 410 | 240 | 240 | n/a[b] | n/a[b] | n/a[b] |
| His-on | 2.001 | 2.235 | 2.275 | 305 | 40 | 30 | 60 | 10 | 10 |
| (C) Co(II)Cbi$^+$/*Se*CobA$^{F91H}$/ATP | 2.002 | 2.235 | 2.280 | 280 | 40 | 30 | 52 | 10 | 10 |
| (D) Co(II)Cbl | 2.001 | 2.235 | 2.275 | 305 | 40 | 30 | 60 | 10 | 10 |

[a]Values for free Co(II)Cbl are also shown for comparison. [b]Not applicable.

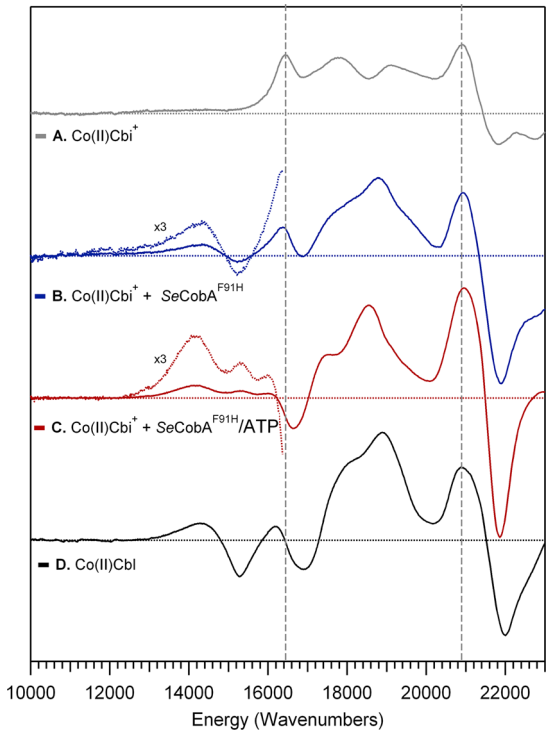


**Figure 9.** MCD spectra collected at 4.5 K and 7 T of (A) free Co(II)Cbi$^+$, (B) Co(II)Cbi$^+$ in the presence of *Se*CobA, and (C) Co(II)Cbi$^+$ in the presence of *Se*CobA and ATP. For reference, the spectrum of free Co(II)Cbl is shown in panel D. The most intense features of free Co(II)Cbi$^+$ are highlighted by dashed vertical lines. The lower-energy region of the spectra of protein-bound species is scaled by a factor of 3 to highlight unique features in this region.

acid substitutions on the Co(II)rrinoid−*Se*CobA interaction. As this enzyme is tasked with (i) binding the ATP and Co(II)rrinoid cosubstrates, (ii) Co(II)rrinoid reduction, and (iii) directing nucleophilic attack of the highly reactive Co(I) intermediate toward the 5′-carbon of ATP, the particular step that is affected by a given substitution is unclear from kinetic studies alone.

**Effects of Amino Acid Substitutions on the 5c → 4c Co(II)rrinoid Conversion Yield and Co−C(Ado) Bond Formation.** The $K_M$ values established from recent kinetic studies of *Se*CobA$^{WT}$ can be compared to the relative yields of formation of 4c Co(II)Cbl established by our MCD experiments (see the Supporting Information for details)[30] to determine whether a given amino acid substitution at the active site of *Se*CobA$^{WT}$ mainly affects the Co(II)/Co(I) reduction step or the subsequent nucleophilic attack of the transiently generated Co(I) species on cosubstrate ATP. Because 4c Co(II)rrinoid formation is a prerequisite for generating the Co(I) "supernucleophile", changes to the 5c−4c Co(II)rrinoid equilibrium should correlate with enzymatic activity provided that the 5c → 4c Co(II)rrinoid conversion contributes to the rate-limiting step. As summarized in Table 4 (right columns), a correlation indeed exists between changes in enzymatic activity caused by amino acid substitutions and the relative yield of 4c Co(II)rrinoid, indicating that the reduced activity of the variants is largely due to perturbations to the Co(II)/Co(I) reduction step. While the 8% relative yield of 4c Co(II)Cbl determined by our MCD studies of *Se*CobA$^{WT}$ is smaller than the value of 25% estimated from the corresponding $K_M$ value (see the Supporting Information for details), the dramatic increase in the relative yield of formation of 4c Co(II)Cbl observed spectroscopically with *Se*CobA$^{F91Y}$ correlates well with the kinetic data. Similarly, the lower 4c Co(II)Cbl yields achieved by the *Se*CobA$^{W93H}$ and *Se*CobA$^{W93F/F91W}$ variants relative to that of *Se*CobA$^{WT}$ are consistent with the $K_M$ values determined for these variants.

The most recently reported crystal structure of *Se*CobA in the presence of Co(II)Cbl and MgATP indicates that residues W93 and F91, which are critical for 4c Co(II)rrinoid formation in the active site of *Se*CobA$^{WT}$, remain partially solvent exposed in the "closed" conformation (Figure 10). Our spectroscopic results do not preclude the possibility that subtle changes in the solvation environment could affect the organization of the active site of *Se*CobA, in particular with respect to the burial of the F91 and W93 side chains, and thus the activity of the enzyme.[60,61] However, given the general agreement between our spectroscopic data and published kinetic results, it appears that these changes, if present, have relatively minor effects on the activity of *Se*CobA variants under physiological conditions.

Differences between the relative yields of 4c Co(II)rrinoids estimated on the basis of $K_M$ values and observed by MCD

Table 3. Kinetic Parameters for the Adenosylation of Co(II)Cbl and Co(II)Cbi$^+$ by *Se*CobA$^{WT}$

| | corrinoid | | | ATP | | |
|---|---|---|---|---|---|---|
| species | $K_M$ ($\mu$M) | $k_{cat}$ ($s^{-1}$) | $k_{cat}/K_M$ ($M^{-1}$ $s^{-1}$) | $K_M$ ($\mu$M) | $k_{cat}$ ($s^{-1}$) | $k_{cat}/K_M$ ($M^{-1}$ $s^{-1}$) |
| Co(II)Cbi$^+$ | 16.3 ± 3.5 | (7.7 ± 0.4) × $10^{-3}$ | (4.7 ± 0.6) × $10^2$ | 25.4 ± 9.0 | (6.7 ± 0.7) × $10^{-3}$ | (2.6 ± 0.4) × $10^2$ |
| Co(II)Cbl[a] | 25 ± 5 | (6.0 ± 0.9) × $10^{-3}$ | (2.0 ± 0.4) × $10^2$ | 66 ± 18 | (5.0 ± 0.7) × $10^{-3}$ | (0.8 ± 0.2) × $10^2$ |

[a]From ref 34.


dx.doi.org/10.1021/bi5011877 | *Biochemistry* 2014, 53, 7969−7982

**Table 4. Positions of the δ-Band in the MCD Spectra of 4c Co(II)Cbi$^+$ and Co(II)Cbl Generated in the Active Sites of *Se*CobA$^{WT}$ and Several Variants[a]**

| | Co(II)Cbi$^+$ | | | Co(II)Cbl | | | |
|---|---|---|---|---|---|---|---|
| *Se*CobA substitution | $\nu(\delta)$ (cm$^{-1}$) | $\Delta\nu(\delta)$ (cm$^{-1}$) | 4c yield (%) | $\nu(\delta)$ (cm$^{-1}$) | $\Delta\nu(\delta)$ (cm$^{-1}$) | 4c yield (%) | expected yield (%) |
| (A) none (WT) | 12270 | 0 | 50 | 12350 | 80 | 8 | 25 |
| (B) F91W | 12230 | −40 | 85 | 12260 | −10 | 7 | 4 |
| (C) F91Y | 12300 | 30 | >95 | 12320 | 50 | 40 | 45 |
| (D) W93F | 12240 | −30 | 89 | 12220 | −50 | 2 | 68 |
| (E) W93H | 12180 | −90 | 41 | n/a[b] | n/a[b] | n/d[c] | 19 |
| (F) W93F/F91W | 12210 | −60 | 5 | n/a[b] | n/a[b] | n/d[c] | 20 |
| (G) W93A | n/a[b] | n/a[b] | n/d[c] | n/a[b] | n/a[b] | n/d[c] | n/a[b] |

[a]Shifts in the δ-band are shown in relation to the position of this feature in the spectrum of Co(II)Cbi$^+$ in the presence of the *Se*CobA$^{WT}$/ATP complex. Also shown are the relative yields of 4c species estimated from the δ-band intensities. The expected yields based on kinetic results obtained with Co(II)Cbl are also shown (see the Supporting Information for details)[34]. [b]Not applicable. [c]Not detected.

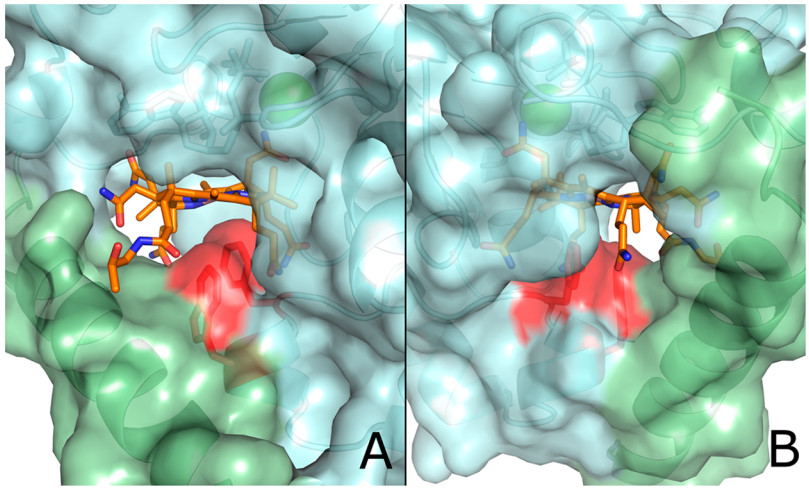


**Figure 10.** Surface representation of the Co(II)Cbl binding site in the "closed" conformation of *Se*CobA based on PDB entry 4HUT. In panel A, the protein is oriented as in Figure 3, while in panel B, the backside of the active site is shown. Contributions from the F91 and W93 residues are colored red to highlight the exposure of these residues to solvent.

spectroscopy could also arise from perturbations to the Co−C(Ado) bond formation step, e.g., via alterations in the relative positioning of the Co(I)rrinoid intermediate and the adenosyl moiety of ATP. While changes to both the 5c → 4c Co(II)rrinoid conversion yield and the Co−C(Ado) bond formation step likely contribute to the altered catalytic rates of the *Se*CobA variants investigated, our spectroscopic data suggest that the latter is the predominant contributor when F91 is replaced with a Trp residue. The F91W substitution significantly increases the bulk of the protein scaffold below the Coβ face of the corrin ring (Table 5) and thus is expected to introduce steric crowding into the "closed" conformation. Consistent with this prediction, the MCD spectra of Co(II)Cbi$^+$ in the presence of *Se*CobA$^{F91W}$ and *Se*CobA$^{WT}$ show considerable differences (Figure 6). Hence, even though the relative yield of 4c Co(II)rrinoid achieved by *Se*CobA$^{F91W}$ is high, this variant displays little catalytic activity. When the F91W substitution is paired with the W93F substitution to mitigate this steric clash, the catalytic activity increases substantially, despite the fact that the fraction of 4c Co(II)rrinoid in the *Se*CobA$^{W93F/F91W}$ variant is much smaller than in *Se*CobA$^{F91W}$. Thus, while maximizing the yield of 4c Co(II)rrinoid species is critical for high catalytic activity, careful control of the positioning of the corrinoid substrate in the active site of *Se*CobA is also important for catalysis.

**Table 5. DFT-Computed Relative Dispersion Energies ($\Delta E_{D3}$) for Different Pairs of Amino Acid Residues in the Active Site of *Se*CobA$^{WT}$ and Several Variants in the "Closed" Conformations and Estimated Free Energy Changes for the Equilibrium between the 4c and 5c States of the Co(II)Cbl and Co(II)Cbi$^+$ Substrates ($\Delta\Delta G_{4c}$) Based on the 5c → 4c Co(II)rrinoid Conversion Yields from Table 4[a]**

| | | | | $\Delta\Delta G_{4c}$ (kJ/mol) | |
|---|---|---|---|---|---|
| *Se*CobA substitution | active-site model | $\Delta E_{D3}$ (kJ/mol) | ΔSA (Å$^2$) | Co(II)Cbi$^+$ | Co(II)Cbl |
| W93A | Phe, Ala | 115 | −56.7 | ≫9 | ≫9 |
| W93H | Phe, His | 64 | −34.7 | 0.74 | 8.98 |
| W93F | Phe, Phe | 40 | −17.9 | −4.2 | 7.7 |
| *W93F/F91W* | *Trp, Phe* | *17* | *27.2* | *5.7* | *>9* |
| **WT** | **Phe, Trp** | **0** | **0.0** | **0.00** | **4.60** |
| F91Y | Try, Trp | −13 | 8.5 | −5.79 | 0.82 |
| *F91W* | *Trp, Trp* | *−39* | *48.5* | *−3.37* | *5.09* |

[a]The change in solvent accessible surface area (ΔSA) for each pair of residues in the absence of the protein is provided as a measure of the bulkiness of each pair. All values are shown in relation to Co(II)Cbi$^+$ bound to the *Se*CobA$^{WT}$/ATP complex (bold). Cases in which the ΔSA values are >27 Å$^2$ are highlighted in italics.

Our MCD spectra also provide insight into the geometry adopted by the Co(II)Cbl substrate in the "open" conformation


dx.doi.org/10.1021/bi5011877 | *Biochemistry* 2014, 53, 7969−7982

of *Se*CobA, prior to removal of the DMB moiety. A comparison of the MCD features exhibited by free Co(II)Cbl and of the 5c Co(II)Cbl species in the presence of the different *Se*CobA/ATP complexes investigated reveals small but noticeable differences. In particular, the decrease in the intensity of the negatively signed band at ~15 000 $cm^{-1}$, along with the minor red-shift of the positive feature at ~17000 $cm^{-1}$ observed for *Se*CobA$^{WT}$ and all variants except for *Se*CobA$^{W93A}$ (Figure 7), indicates that the 5c Co(II)Cbl fraction is enzyme-bound, with a perturbed Co−N(DMB) bonding interaction. This finding is consistent with the crystal structure of *Se*CobA$^{WT}$, which revealed that in the "open" conformation, residue W93 is spatially very close to the ribose moiety that makes up part of the nucleotide loop of Co(II)Cbl. This steric clash may contribute to the elongated Co−N(DMB) bond of the 5c Co(II)Cbl species observed in the X-ray crystal structure of *Se*CobA$^{WT}$ (see Table 1). As the nearby F91 side chain is properly positioned to participate in a $\pi$-stacking interaction with residue W93 in the "open" conformation, substitution of F91 would be expected to introduce further perturbations into the Co−N(DMB) bond of enzyme-bound Co(II)Cbl, consistent with our MCD data. Thus, we conclude that in the "open" conformation of *Se*CobA$^{WT}$, the F91 and W93 residues are positioned so as to weaken the Co−N(DMB) bond via steric interactions with the bulky DMB moiety.

**Mechanism of 4c Co(II)rrinoid Formation.** Because MCD spectroscopy provides a uniquely sensitive tool for discriminating between 4c and 5c Co(II)rrinoids, it is possible to use our data as the basis for estimating the change in free energy for the formation of 4c species in response to active-site amino acid substitutions, $\Delta\Delta G_{4c}$ (see the Supporting Information for details). Using Co(II)Cbi$^+$ bound to the *Se*CobA$^{WT}$/ATP complex as the reference point, our analysis yields a range of $\Delta\Delta G_{4c}$ values between −6 and 9 kJ/mol based on the detection limit of 4c Co(II)rrinoid species by our MCD instrument [~1% relative to the entire population of Co(II)-rrinoids]. On average, $\Delta\Delta G_{4c}$ increases by ~8 kJ/mol when Co(II)Cbl instead of Co(II)Cbi$^+$ is used as the substrate (Table 4, right columns), which can be attributed to the increased strength of the Co−N(DMB) bond relative to that of the Co−O($H_2$) bond. The increase in Co−N(DMB) bond strength estimated from our results is consistent with the 40-fold decrease in $K_M$ values previously observed for the binding of AdoCbl to MMCM (which binds AdoCbl in a base-off, His-on fashion)[3] relative to hATR (which excludes the binding of axial ligands to the Co$\alpha$ face of the corrin ring where the DMB group would usually be found).[21,37,62] However, this difference is not constant across the entire series of *Se*CobA variants investigated, because specific, species-dependent intermolecular interactions between the protein side chains and the DMB moiety are likely important for promoting Co−N(DMB) bond dissociation (*vide supra*). The fact that *Se*CobA$^{WT}$ achieves a higher 5c → 4c conversion yield with Co(II)Cbi$^+$ as the substrate is consistent with its main role in the adenosylation of incomplete corrinoids that generally lack the nucleotide loop and terminal DMB base.

A comparison of the "open" and "closed" conformations observed in the crystal structure of *Se*CobA$^{WT}$ complexed with Co(II)Cbl and MgATP reveals only minor differences in the vicinity of the Co$\beta$ face of the corrin ring that is oriented toward cosubstrate ATP. In contrast, large conformational differences exist near the Co$\alpha$ face of the corrin ring, in particular with regard to residues F91 and W93 that move by ~12.1 and ~7.5 Å, respectively, relative to their solvent-exposed positions in the "open" conformation, to fill the space originally occupied by the DMB moiety. Given the size and hydrophobicity of these residues, as well as their positioning in an offset $\pi$-stacking configuration in the "closed" conformation, it is likely that dispersion interactions play a role in stabilizing the "closed" over the "open" conformation of *Se*CobA.[63,64] To evaluate this possibility, the magnitude of dispersion interactions involving residues 91 and 93 was estimated by DFT computations (see Materials and Methods for details). Inspection of the computed relative dispersion energies, $\Delta E_{D3}$, for various combinations of residues reveals a correlation between these values and the relative population of 4c Co(II)Cbi$^+$ generated in the different *Se*CobA variants investigated (Table 4). While the computed $\Delta E_D$ values are generally much larger than the dispersion energies reported for related model systems,[63,65] they properly reproduce the experimental trends and correlate well with the size of the interacting $\pi$-systems.[66] Consistent with the inability of *Se*CobA$^{W93A}$ to convert Co(II)Cbl and Co(II)Cbi$^+$ to 4c species and the lack of catalytic activity displayed by this variant, the computed $E_D$ value for the Phe-Ala fragment is 115 kJ/mol smaller than that obtained for the Phe-Trp fragment present in *Se*CobA$^{WT}$, highlighting the importance of the F91 residue in stabilizing the "closed" conformation of the protein. A largely reduced $E_D$ value (by ~64 kJ/mol) is also predicted for the Phe-His pair, consistent with our spectroscopic data for *Se*CobA$^{W93H}$, which indicate that this variant is relatively ineffective at converting Co(II)Cbi$^+$ to a 4c species and fails to promote dissociation of the DMB group from Co(II)Cbl. Finally, replacement of Phe with Tyr, a polar aromatic residue, results in a modest (~13 kJ/mol) increase in the computed $E_D$ value, in qualitative agreement with the higher relative 4c Co(II)rrinoid yields observed experimentally for the *Se*CobA$^{F91Y}$ variant.

The $E_D$ values obtained for the remaining active-site models agree less well with the experimental trends, supporting our hypothesis that additional factors affect the 5c → 4c Co(II)rrinoid conversion yield (*vide supra*). As our spectroscopic results reveal a uniquely perturbed conformation of the Co(II)rrinoid substrate in the *Se*CobA variants possessing the F91W substitution (*Se*CobA$^{F91W}$ and *Se*CobA$^{F91W,W93F}$), it is worth noting that the introduction of the larger indole moiety dramatically increases the bulkiness of the active site, as indicated by the >27 $Å^2$ increase in the solvent accessible surface area (ΔSA) of paired residues 91 and 93 in these variants (Table 5). Thus, it is likely that our simple models do not properly account for all of the changes in protein conformation that are needed to accommodate the larger residues. Similar factors may contribute to the poor agreement between the computed $E_D$ value and the relative yield of 4c Co(II)rrinoid formation in the case of *Se*CobA$^{W93F}$.

Despite certain exceptions to the general trend in the $E_D$ values, our computational results provide strong evidence that favorable enthalpic contributions from offset $\pi$-stacking interactions between residues 91 and 93 in the "closed" conformation of *Se*CobA contribute to 4c Co(II)rrinoid formation. In addition, our results indicate that in the absence of a bulky, planar residue, as in the case of *Se*CobA$^{W93A}$, steric interactions needed for axial ligand exclusion no longer exist, possibly allowing solvent molecules to interact with the corrin ring, as shown by the essentially unperturbed conformation of Co(II)rrinoids in the presence of this variant. Similarly, the


dx.doi.org/10.1021/bi5011877 | *Biochemistry* 2014, 53, 7969−7982

introduction of smaller aromatic residues (as in *Se*CobA$^{W93F}$ and *Se*CobA$^{W93H}$) likely diminishes the conformational rigidity of the active site, consistent with the broadening of the $\delta$-band in the corresponding MCD spectra (Figure 6, traces D and E), while introduction of larger residues results in significant steric strain that may cause distortions of the corrin ring, as observed for *Se*CobA$^{F91W}$. Furthermore, our experimental and computational results indicate that the replacement of a hydrogen atom in the F91 side chain with a hydroxyl group does not result in large changes in the conformation of the active site. However, it does increase the number of dispersion interactions with the nearby W93 residue, thus stabilizing the "closed" conformation. The calculated ~13 kJ/mol increase in $E_D$ is on the order of our experimentally estimated difference in $\Delta\Delta G_{4c}$ of ~8 kJ/mol for the dissociation of the DMB moiety from Co(II)Cbl versus $H_2O$ dissociation from Co(II)Cbi$^+$ (*vide supra*), indicating that this contribution alone may be sufficient to account for the dramatic increase in the 4c Co(II)Cbl yield achieved by *Se*CobA$^{F91Y}$.

**Implications for the Mechanism of Co(II)rrinoid Reduction and Adenosylation *in Vivo*.** Crystallographic studies revealed that binding of ATP to *Se*CobA$^{WT}$ causes the active site to adopt a conformation in which it can engage in dipolar interactions with the acetamide and propionamide side chains on the corrin ring and thus facilitate the binding of the Co(II)rrinoid substrate.[34,36] In this "open" conformation of *Se*CobA$^{WT}$, the lower axial ligand (either DMB or $H_2O$) remains associated with the Co(II) ion but likely interacts with the nearby W93 residue. Further structural changes to the active-site structure occur upon formation of the "closed" conformation, in particular to the N-terminal region of the adjacent subunit as well as the segment between residues M87 and C105, which adopt helical structures. As a result, the Co(II)rrinoid substrate shifts ~0.3 Å closer to the 5′-carbon of ATP while the F91 and W93 residues move below the Co$\alpha$ face of the corrin ring to generate a unique 4c Co(II)rrinoid species. While the "open" and "closed" conformations of the enzyme exist in an equilibrium, it is only in the "closed" conformation where the required tuning of the Co(II)/Co(I) reduction potential occurs via elimination of any axial ligand interactions. As evidenced by the spectroscopic data obtained in this study, the equilibrium between these conformations depends on the nature of the axial ligand of the bound Co(II)rrinoid and is sensitive to amino acid substitutions in the active site of *Se*CobA. Collectively, our data indicate that the "closed" conformation is stabilized over the "open" conformation by hydrophobic effects, as observed for the related *Lr*PudO ACAT, and by $\pi$-stacking interactions between residues F91 and W93.

In the X-ray crystal structure of *Se*CobA$^{WT}$, the distance between the Co(II) ion of the 4c fraction of Co(II)Cbl and the 5′-carbon of cosubstrate ATP is ~3.0 Å, which is only ~1.0 Å larger than the Co−C(Ado) bond distance in AdoCbl.[3] As this 4c fraction of Co(II)Cbl is activated for one-electron reduction by flavins to produce a "supernucleophilic" Co(I)rrinoid species, the proximity of the two substrates is critical for avoiding undesired side reactions. The positioning of the corrinoid relative to the cosubstrate ATP is likely controlled, at least in part, by the conformation of the M87−C105 loop. In support of this hypothesis, *Se*CobA$^{F91W}$ displays a drastically diminished catalytic activity because of the misalignment of the corrinoid substrate, even though it achieves wild-type-like relative yields of formation of 4c Co(II)Cbl and Co(II)Cbi$^+$. These findings highlight the delicate balance of interactions that must be present in the active site of *Se*CobA for the formation of 4c Co(II)rrinoids. Our findings also provide clues about why *Ralstonia* species express CobA with Tyr at position 91 in lieu of the Phe present in *Se*CobA.[34] While *in vivo* *Se*CobA is responsible for the adenosylation of a variety of corrinoid substrates,[10] our results indicate that Co(II)Cbl provides a significant challenge for this enzyme, as only ~8% of Co(II)Cbl is converted to a 4c species. Substitution of F91 with a Tyr residue increases the amount of 4c species generated from Co(II)Cbl 5-fold. It is possible that these homologous CobAs with active-site tyrosines have been selected for *in vivo* conditions that demand a very high rate of turnover of AdoCbl, or perhaps these organisms are "fed" cobalamin by mutualistic strains and no longer need to process cobinamide. Another possibility is that the active-site tyrosine is more effective at generating 4c species of cobamides that possess Co$\beta$ ligands other than DMB, which could include one of several types of purines, phenolics, or DMB derivatives.[40] The *in vitro* effectiveness of *Se*CobA$^{WT}$ to adenosylate alternative cobamides has yet to be determined.

## ■ ASSOCIATED CONTENT

### Ⓢ Supporting Information

Additional details regarding the preparation of samples, absorption data, and equations and strategy used to evaluate $\Delta\Delta G_{4c}$ values and relative yields of 4c Co(II)rrinoids. This material is available free of charge via the Internet at http://pubs.acs.org.

## ■ AUTHOR INFORMATION


### Corresponding Author

*Address: 1101 University Ave., Madison, WI 53706. E-mail: brunold@chem.wisc.edu. Phone: (608) 265-9056. Fax: (608) 262-6143.



### Funding

This work was supported in part by National Science Foundation Grants MCB-0238530 (to T.C.B.) and CHE-0840494. I.G.P. was supported in part by Grant 5T32GM08349 via the Biotechnology Training Grant at the University of Wisconsin—Madison. T.C.M. was supported in part by National Institutes of Health Grant T32 GM008505 (Chemistry and Biology Interface Training Grant) and by National Institutes of Health Grant R37-GM40313 to J.C.E.-S.


### Notes

The authors declare no competing financial interest.

## ■ ADDITIONAL NOTE

[a]$\theta$(LA) is the angle between the plane containing the $N_A$, $C_4$−$C_6$, and $N_B$ atoms and the plane containing the $N_C$, $C_{14}$−$C_{16}$, and $N_D$ atoms, while $\phi$(SA) corresponds to the angle between the planes containing the $N_D$, $C_{19}$, $C_1$, and $N_A$ atoms and the $N_B$, $C_9$−$C_{11}$, and $N_C$ atoms (see Figure S8 of the Supporting Information for the atom numbering scheme used).

## ■ REFERENCES


(1) Toraya, T. (2014) Cobalamin-dependent dehydratases and a deaminase: Radical catalysis and reactivating chaperones. *Arch. Biochem. Biophys. 544*, 40−57.

(2) Marsh, E. N. G., Patterson, D. P., and Li, L. (2010) Adenosyl radical: Reagent and catalyst in enzyme reactions. *ChemBioChem 11*, 604−621.

(3) Randaccio, L., Geremia, S., Demitri, N., and Wuerges, J. (2010) Vitamin B-12: Unique metalorganic compounds and the most complex vitamins. *Molecules 15*, 3228−3259.
(4) *Enzyme-Catalyzed Electron and Radical Transfer*, Vol. 35 (2000) Kluwer Academic Publishers, New York.
(5) Shibata, N., Masuda, J., Tobimatsu, T., Toraya, T., Suto, K., Morimoto, Y., and Yasuoka, N. (1999) A new mode of $B_{12}$ binding and the direct participation of a potassium ion in enzyme catalysis: X-ray structure of diol dehydratase. *Structure (Oxford, U.K.) 7*, 997−1008.
(6) Abend, A., Bandarian, V., Nitsche, R., Stupperich, E., Retey, J., and Reed, G. H. (1999) Ethanolamine ammonia-lyase has a "base-on" binding mode for coenzyme $B_{12}$. *Arch. Biochem. Biophys. 370*, 138−141.
(7) Frey, P. A., and Chang, C. H. (1999) *Aminomutases, in Chemistry and Biochemistry of $B_{12}$*, John Wiley & Sons, Inc., New York.
(8) Ludwig, M. L., and Matthews, R. G. (1997) Structure-based perspectives on $B_{12}$-dependent enzymes. *Annu. Rev. Biochem. 66*, 269−313.
(9) Marsh, E. N. G., and Ballou, D. P. (1998) Coupling of cobalt-carbon bond homolysis and hydrogen atom abstraction in adenosylcobalamin-dependent glutamate mutase. *Biochemistry 37*, 11864−11872.
(10) Warren, M. J., Raux, E., Schubert, H. L., and Escalante-Semerena, J. C. (2002) The biosynthesis of adenosylcobalamin (vitamin B-12). *Nat. Prod. Rep. 19*, 390−412.
(11) Mera, P. E., and Escalante-Semerena, J. C. (2010) Multiple roles of ATP:cob(I) alamin adenosyltransferases in the conversion of $B_{12}$ to coenzyme $B_{12}$. *Appl. Microbiol. Biotechnol. 88*, 41−48.
(12) Escalante-Semerena, J. C., Suh, S. J., and Roth, J. R. (1990) CobA function is required for both *de novo* cobalamin biosynthesis and assimilation of exogenous corrinoids in *Salmonella typhimurium*. *J. Bacteriol. 172*, 273−280.
(13) Johnson, C. L. V., Buszko, M. L., and Bobik, T. A. (2004) Purification and initial characterization of the *Salmonella enterica* PduO ATP:cob(I)alamin adenosyltransferase. *J. Bacteriol. 186*, 7881−7887.
(14) Buan, N. R., Suh, S. J., and Escalante-Semerena, J. C. (2004) The eutT gene of *Salmonella enterica* encodes an oxygen-labile, metal-containing ATP:corrinoid adenosyltransferase enzyme. *J. Bacteriol. 186*, 5708−5714.
(15) Mera, P. E., Maurice, M. S., Rayment, I., and Escalante-Semerena, J. C. (2007) Structural and functional analyses of the human-type corrinoid adenosyltransferase (PduO) from *Lactobacillus reuteri*. *Biochemistry 46*, 13829−13836.
(16) Buan, N. R., Suh, S. J., and Escalante-Semerena, J. C. (2004) The eutT gene of *Salmonella enterica* encodes an oxygen-labile, metal-containing ATP:corrinoid adenosyltransferase enzyme (vol 186, pg 5711, 2004). *J. Bacteriol. 186*, 7826.
(17) Buan, N. R., and Escalante-Semerena, J. C. (2006) Purification and initial biochemical characterization of ATP:cob(I)alamin adenosyltransferase (EutT) enzyme of *Salmonella enterica*. *J. Biol. Chem. 281*, 16971−16977.
(18) Park, K. (2010) Spectroscopic and computational insights into the mechanism employed by adenosyltrasferases for coenzyme-$B_{12}$ biosynthesis. Ph.D. Thesis, University of Wisconsin—Madison, Madison, WI.
(19) Banerjee, R. (2001) Radical peregrinations catalyzed by $B_{12}$ enzymes. *Biochemistry 40*, 6191−6198.
(20) Jorge-Finnigan, A., Aguado, C., Sanchez-Alcudia, R., Abia, D., Richard, E., Merinero, B., Gamez, A., Banerjee, R., Desviat, L. R., Ugarte, M., and Perez, B. (2010) Functional and structural analysis of five mutations identified in methylmalonic aciduria cblB Type. *Hum. Mutat. 31*, 1033−1042.
(21) Padovani, D., Labunska, T., Palfey, B. A., Ballou, D. P., and Banerjee, R. (2008) Adenosyltransferase tailors and delivers coenzyme $B_{12}$. *Nat. Chem. Biol. 4*, 194−196.
(22) Fonseca, M. V., and Escalante-Semerena, J. C. (2000) Reduction of cob(III)alamin to cob(II)alamin in *Salmonella enterica serovar typhimurium* LT2. *J. Bacteriol. 182*, 4304−4309.
(23) Liptak, M. D., and Brunold, T. C. (2006) Spectroscopic and computational studies of $Co^{1+}$ cobalamin: Spectral and electronic properties of the "superreduced" $B_{12}$ cofactor. *J. Am. Chem. Soc. 128*, 9144−9156.
(24) Stich, T. A., Buan, N. R., Escalante-Semerena, J. C., and Brunold, T. C. (2005) Spectroscopic and computational studies of the ATP:corrinoid adenosyltransferase (CobA) from *Salmonella enterica*: Insights into the mechanism of adenosylcobalamin biosynthesis. *J. Am. Chem. Soc. 127*, 8710−8719.
(25) Lexa, D., and Saveant, J. M. (1983) The electrochemistry of vitamin $B_{12}$. *Acc. Chem. Res. 16*, 235−243.
(26) Buan, N. R., and Escalante-Semerena, J. C. (2005) Computer-assisted docking of flavodoxin with the ATP:Co(I)rrinoid adenosyltransferase (CobA) enzyme reveals residues critical for protein-protein interactions but not for catalysis. *J. Biol. Chem. 280*, 40948−40956.
(27) Hoover, D. M., Jarrett, J. T., Sands, R. H., Dunham, W. R., Ludwig, M. L., and Matthews, R. G. (1997) Interaction of *Escherichia coli* cobalamin-dependent methionine synthase and its physiological partner flavodoxin: Binding of flavodoxin leads to axial ligand dissociation from the cobalamin cofactor. *Biochemistry 36*, 127−138.
(28) Olteanu, H., Wolthers, K. R., Munro, A. W., Scrutton, N. S., and Banerjee, R. (2004) Kinetic and thermodynamic characterization of the common polymorphic variants of human methionine synthase reductase. *Biochemistry 43*, 1988−1997.
(29) Park, K., Mera, P. E., Escalante-Semerena, J. C., and Brunold, T. C. (2008) Kinetic and spectroscopic studies of the ATP:corrinoid adenosyltransferase PduO from *Lactobacillus reuteri*: Substrate specificity and insights into the mechanism of Co(II)corrinoid reduction. *Biochemistry 47*, 9007−9015.
(30) Park, K., Mera, P. E., Escalante-Semerena, J. C., and Brunold, T. C. (2012) Spectroscopic Characterization of Active-Site Variants of the PduO-type ATP:Corrinoid Adenosyltransferase from *Lactobacillus reuteri*: Insights into the Mechanism of Four-Coordinate Co(II)-corrinoid Formation. *Inorg. Chem. 51*, 4482−4494.
(31) Stich, T. A., Yamanishi, M., Banerjee, R., and Brunold, T. C. (2005) Spectroscopic evidence for the formation of a four-coordinate $Co^{2+}$ cobalamin species upon binding to the human ATP: Cobalamin adenosyltransferase. *J. Am. Chem. Soc. 127*, 7660−7661.
(32) Brunold, T. C., Conrad, K. S., Liptak, M. D., and Park, K. (2009) Spectroscopically validated density functional theory studies of the $B_{12}$ cofactors and their interactions with enzyme active sites. *Coord. Chem. Rev. 253*, 779−794.
(33) St Maurice, M., Mera, P. E., Taranto, M. P., Sesma, F., Escalante-Semerena, J. C., and Rayment, I. (2007) Structural characterization of the active site of the PduO-type ATP:Co(I)rrinoid adenosyltransferase from *Lactobacillus reuteri*. *J. Biol. Chem. 282*, 2596−2605.
(34) Moore, T. C., Newmister, S. A., Rayment, I., and Escalante-Semerena, J. C. (2012) Structural insights into the mechanism of four-coordinate cob(II)alamin formation in the active site of the *Salmonella enterica* ATP:Co(I)rrinoid adenosyltransferase enzyme: Critical role of residues Phe91 and Trp93. *Biochemistry 51*, 9647−9657.
(35) Mera, P. E., St Maurice, M., Rayment, I., and Escalante-Semerena, J. C. (2009) Residue Phe112 of the human-type corrinoid adenosyltransferase (PduO) enzyme of *Lactobacillus reuteri* is critical to the formation of the four-coordinate Co(II) corrinoid substrate and to the activity of the enzyme. *Biochemistry 48*, 3138−3145.
(36) Bauer, C. B., Fonseca, M. V., Holden, H. M., Thoden, J. B., Thompson, T. B., Escalante-Semerena, J. C., and Rayment, I. (2001) Three-dimensional structure of ATP:corrinoid adenosyltransferase from *Salmonella typhimurium* in its free state, complexed with MgATP, or complexed with hydroxycobalamin and MgATP. *Biochemistry 40*, 361−374.
(37) St Maurice, M., Mera, P., Park, K., Brunold, T. C., Escalante-Semerena, J. C., and Rayment, I. (2008) Structural characterization of a human-type corrinoid adenosyltransferase confirms that coenzyme $B_{12}$ is synthesized through a four-coordinate intermediate. *Biochemistry 47*, 5755−5766.
(38) Stich, T. A., Buan, N. R., and Brunold, T. C. (2004) Spectroscopic and computational studies of $Co^{2+}$ corrinoids: Spectral

and electronic properties of the biologically relevant base-on and base-off forms of $Co^{2+}$ cobalamin. *J. Am. Chem. Soc. 126*, 9735−9749.
(39) Liptak, M. D., Fleischhacker, A. S., Matthews, R. G., Telser, J., and Brunold, T. C. (2009) Spectroscopic and computational characterization of the base-off forms of cob(II)alamin. *J. Phys. Chem. B 113*, 5245−5254.
(40) IUPAC-IUB Commission on Biochemical Nomenclature (1974) Nomenclature of corrinoids (1973 recommendations). IUPAC-IUB commission on biochemical nomenclature. *Biochemistry 13*, 1555−1560.
(41) Johnson, M. G., and Escalante-Semerena, J. C. (1992) Identifycation of 5,6-dimethylbenzymidazole as the Co$\alpha$ ligand of the cobamide synthesized by *Salmonella typhimurium*. Nutritional characterization of mutants defective in biosynthesis of the imidazole ring. *J. Biol. Chem. 267*, 13302−13305.
(42) Rocco, C. J., Dennison, K. L., Klenchin, V. A., Rayment, I., and Escalante-Semerena, J. C. (2008) Construction and use of new cloning vectors for the rapid isolation of recombinant proteins from *Escherichia coli*. *Plasmid 59*, 231−237.
(43) Blommel, P. G., and Fox, B. G. (2007) A combined approach to improving large-scale production of tobacco etch virus protease. *Protein Expression Purif. 55*, 53−68.
(44) Laemmli, U. K. (1970) Cleavge of structural proteins during assembly of head of bacteriophage-T4. *Nature 227*, 680−685.
(45) Berendsen, H. J. C., Postma, J. P. M., van Gunsteren, W. F., and Hermans, J. (1981) *Intermolecular Forces*; Reidel Publishing Co., Dordrecht, The Netherlands.
(46) Meagher, K. L., Redman, L. T., and Carlson, H. A. (2003) Development of polyphosphate parameters for use with the AMBER force field. *J. Comput. Chem. 24*, 1016−1025.
(47) Marques, H. M., Ngoma, B., Egan, T. J., and Brown, K. L. (2001) Parameters for the AMBER force field for the molecular mechanics modeling of the cobalt corrinoids. *J. Mol. Struct. 561*, 71−91.
(48) Marsh, E. N. G., and Melendez, G. D. R. (2012) Adenosylcobalamin enzymes: Theory and experiment begin to converge. *Biochim. Biophys. Acta 1824*, 1154−1164.
(49) Brandenburg, J. G., and Grimme, S. (2013) A dispersion-corrected density functional theory case study on ethyl acetate conformers, dimer, and molecular crystal. *Theor. Chem. Acc. 132*, 1399.
(50) Grimme, S., Antony, J., Schwabe, T., and Muck-Lichtenfeld, C. (2007) Density functional theory with dispersion corrections for supramolecular structures, aggregates, and complexes of (bio)organic molecules. *Org. Biomol. Chem. 5*, 741−758.
(51) Grimme, S., Antony, J., Ehrlich, S., and Krieg, H. (2010) A consistent and accurate ab initio parametrization of density functional dispersion correction (DFT-D) for the 94 elements H-Pu. *J. Chem. Phys. 132*, 154104.
(52) Neese, F. (2008) *ORCA-An Ab initio, Density Functional, and Semiempirical Program Package*, version 2.9.1, Universitat Bonn, Bonn, Germany.
(53) Pratt, J. M. (1972) *Inorganic Chemistry of Vitamin B12*, Academic Press Inc., London.
(54) Park, K., and Brunold, T. C. (2013) Combined Spectroscopic and Computational Analysis of the Vibrational Properties of Vitamin $B_{12}$ in its $Co^{3+}$, $Co^{2+}$, and $Co^{1+}$ Oxidation States. *J. Phys. Chem. B 117*, 5397−5410.
(55) Stich, T. A., Brooks, A. J., Buan, N. R., and Brunold, T. C. (2003) Spectroscopic and computational studies of $Co^{3+}$-corrinoids: Spectral and electronic properties of the $B_{12}$ cofactors and biologically relevant precursors. *J. Am. Chem. Soc. 125*, 5897−5914.
(56) Brooks, A. J., Vlasie, M., Banerjee, R., and Brunold, T. C. (2005) Co-C bond activation in methylmalonyl-CoA mutase by stabilization of the post-homolysis product $Co^{2+}$ cobalamin. *J. Am. Chem. Soc. 127*, 16522−16528.
(57) Krautler, B., Keller, W., and Kratky, C. (1989) Coenzyme-$B_{12}$ chemistry: The crystal and moelcular structura of cob(II)alamin. *J. Am. Chem. Soc. 111*, 8936−8938.
(58) Liptak, M. D., Datta, S., Matthews, R. G., and Brunold, T. C. (2008) Spectroscopic study of the cobalamin-dependent methionine synthase in the activation conformation: Effects of the Y1139 residue and S-adenosylmethionine on the $B_{12}$ cofactor. *J. Am. Chem. Soc. 130*, 16374−16381.
(59) Padovani, D., and Banerjee, R. (2009) A rotary mechanism for coenzyme-$B_{12}$ synthesis by adenosyltransferase. *Biochemistry 48*, 5350−5357.
(60) Dias, C. L., Ala-Nissila, T., Karttunen, M., Vattulainen, I., and Grant, M. (2008) Microscopic mechanism for cold denaturation. *Phys. Rev. Lett. 100*, 4.
(61) Dias, C. L., Ala-Nissila, T., Wong-ekkabut, J., Vattulainen, I., Grant, M., and Karttunen, M. (2010) The hydrophobic effect and its role in cold denaturation. *Cryobiology 60*, 91−99.
(62) Banerjee, R., Gherasim, C., and Padovani, D. (2009) The tinker, tailor, soldier in intracellular $B_{12}$ trafficking. *Curr. Opin. Chem. Biol. 13*, 484−491.
(63) Butterfield, S. M., Patel, P. R., and Waters, M. L. (2002) Contribution of aromatic interactions to $\alpha$-helix stability. *J. Am. Chem. Soc. 124*, 9751−9755.
(64) Radzicka, A., and Wolfenden, R. (1988) Comparing the polarities of the amino-acid side chain distribution coefficients between the vapor-phase, cyclohexane, 1-octanol, and neutral aqueous solution. *Biochemistry 27*, 1664−1670.
(65) Gung, B. W., Xue, X. W., and Reich, H. J. (2005) Off-center oxygen-arene interactions in solution: A quantitative study. *J. Org. Chem. 70*, 7232−7237.
(66) Grimme, S. (2008) Do special noncovalent $\pi$-$\pi$ stacking interactions really exist? *Angew. Chem., Int. Ed. 47*, 3430−3434.
(67) Fonseca, M. V., and Escalante-Semerena, J. C. (2001) An in vitro reducing system for the enzymic conversion of cobalamin to adenosylcobalamin. *J. Biol. Chem. 276*, 32101−32108.